LAWRENCE
LIVERMORE
NATIONAL
LABORATORY

UCRL-JRNL-235596

Helium and Neon Abundances and Compositions in Cometary Matter

B. Marty, R. L. Palma, R. O. Pepin, L. Zimmmermann, D. J. Schlutter, P. G. Burnard, A. J. Westphal, C. J. Snead, S. Bajt, R. H. Becker, J. E. Simones

October 17, 2007

Science

Disclaimer

Helium and Neon Abundances and Compositions in Cometary Matter

Bernard Marty[1], Russell L. Palma[2,3], Robert O. Pepin[3]*, Laurent Zimmermann[1], Dennis J. Schlutter[3], Peter G. Burnard[1], Andrew J. Westphal[4], Christopher J. Snead[4], Saša Bajt[5], Richard H. Becker[3], Jacob E. Simones[2]

1: Centre de Recherches Pétrographiques et Géochimiques, BP 20, 54501 Vandoeuvre-lès-Nancy Cedex, France

2: Department of Physics and Astronomy, Minnesota State University, Mankato, MN 56001, USA

3: School of Physics and Astronomy, University of Minnesota, Minneapolis, MN 55455, USA

4: Space Sciences Laboratory, University of California, Berkeley, CA 94720, USA

5: Institute of Geophysics and Planetary Physics, Lawrence Livermore National Laboratory, Livermore, CA 94550, USA

* To whom correspondence should be addressed. E-mail: pepin001@umn.edu

Materials trapped and preserved in comets date from the earliest history of the solar system. Particles captured by the Stardust spacecraft from comet Wild 2 are indisputable cometary matter available for laboratory study. Here we report measurements of noble gases in Stardust material. Neon isotope ratios are within the range observed in "phase Q", a ubiquitous, primitive organic carrier of noble gases in meteorites. Helium displays $^3He/^4He$ ratios twice those in phase Q and in Jupiter's atmosphere. Abundances per gram are surprisingly large, suggesting implantation by ion irradiation. The gases are carried in high temperature igneous grains similar to particles found in other Stardust studies. Collectively the evidence points to gas acquisition in a hot, high ion flux nebular environment close to the young Sun.

Comets are frozen, largely unaltered reservoirs of dust and gases that were present in the early solar nebula. They are likely to contain well-preserved records of the chemical, mineralogic, and isotopic character of primordial solar-system matter. On January 15, 2006, the Stardust Mission returned to Earth with a cargo of particles collected from the coma of comet Wild 2 *(1)*. These not only open the door to detailed laboratory investigation of the nature of cometary matter, but will also provide chemical, mineralogic, and isotopic markers for

identifying samples of comets suspected to be already present in extraterrestrial material collections *(e.g., 2-7)*.

Noble gases are excellent tracers of contributions from various solar system volatile reservoirs and of physical processing of gases acquired from these reservoirs. Their elemental and isotopic compositions in primitive meteorites are different from those in the Sun, as represented by the solar wind. Planetary atmospheres display noble gas signatures distinct from both solar and meteoritic patterns. A detailed knowledge of cometary noble gas abundances and isotopic compositions, unknown prior to Stardust, will allow investigation of compositional links between comets, the solar nebula, primitive meteorites for which a cometary origin has been advocated *(8,9)*, micrometeorites and interplanetary dust particles (IDPs), and the atmospheres of Earth, Mars, and Venus, where contributions of noble gases carried by comets have been proposed and debated *(10-12)*. The isotope ratios and high concentrations of Ne reported here are particularly interesting data for these latter studies.

The Wild 2 particles were collected by Stardust in aerogel, a porous low-density silica glass designed to decelerate an impacting grain with minimal alteration *(1)*. The material analyzed in this study was extracted from the bulbous cavity wall of the capture track shown in Fig. 1A. We report results of helium and neon measurements on five sub-samples of this material (Fig. 1B, and Fig. S1 in *(13)*), carried out independently, using different extraction and analytical methods, at CRPG Nancy, France and the University of Minnesota, Minneapolis, USA *(14)*. Gases were thermally released from the five samples, two (Thera-1 and Thera-2) at CRPG by single-step laser melting and three (St-1, St-2, St-3) at Minnesota by multi-step pyrolysis to ~1400°C. Evolved He and Ne abundances were not large, in some cases exceeding blank levels by factors of only 2-3, and so accurate assessments of aerogel and instrumental blanks were crucial. Details on blank determinations, and other discussions of materials and methods, are set out in *(13)*.

The bulbous track-wall samples are mixtures of aerogel and small grains shed from the impacting particle. Gases were held very retentively in their host grains; temperatures above ~1250°C (± 50°C) were required to degas He and Ne in the Minnesota step-heating procedure. Originally we thought that gases might have been liberated by flash heating of the incident particle in the upper part of its deceleration track (Fig. 1A) and trapped in melted aerogel that rapidly chilled to silica glass along the track walls. It is now clear that the ~1200-1250°C temperatures reached prior to initiation of release *(13)* are incompatible with siting in aerogel.

Diffusion coefficients for He in vitreous silica *(15)* are so large at these temperatures that glassy aerogel would empty itself in ~10 seconds —comparable to step heating times— even if diffusion distances were comparable to the 1 mm sample dimensions (Figs. 1B, S1), and much more quickly (<1 second) at the ≤100 μm scale. Observed release profiles instead point to gas siting in refractory grains. This inference is consistent with the bulb-wall mineralogy measured by x-ray absorption spectroscopy (supporting online text), indicating that the grains are composed primarily (~75% by mass) of high-temperature metal (FeNi), metal-sulphur, and metal-carbon minerals. The remaining 25% are mostly silicates together with unidentified components. A separate search for organic compounds was carried out by infrared spectroscopy to address the possibility that the gas carriers might be refractory organic materials. None were positively detected, setting a low upper limit on their abundances in the bulb wall (supporting online text).

Neon isotopic compositions were measured in both noble gas laboratories. Extractions with enough Ne for relatively precise measurement yielded similar isotope ratios: $^{20}Ne/^{22}Ne = 10.68 \pm 0.35$ and 10.49 ± 0.24 together with $^{21}Ne/^{22}Ne = 0.0273 \pm 0.0024$ and 0.0279 ± 0.0017, measured respectively in St-1 at Minnesota and Thera-2 at CRPG (Table 1). Both $^{20}Ne/^{22}Ne$ ratios are >2.5σ above the atmospheric value of 9.80. These compositions fall within the range observed for meteoritic Ne —specifically, for Ne in "phase Q" *(16),* a minor macromolecular organic phase, ubiquitous in chondritic and achondritic meteorites, that hosts neon with $^{20}Ne/^{22}Ne$ ratios ranging from 10.1 to 10.7, and $^{21}Ne/^{22}Ne$ from a lower limit of 0.0278 to 0.0294 (Table 1). Stardust Ne lies within error in the Ne-Q data field, with the nominal $^{21}Ne/^{22}Ne$ ratios straddling its lower limit (Fig. 2A).

Are there alternatives to a Q-Ne-like source —in particular, a source with solar composition *(17-19)* — that might account for the Ne isotopic distributions within the uncertainties of the present data? The $^{20}Ne/^{22}Ne$ ratio in Thera-1 could be consistent with a solar-wind Ne end-member (Table 1) but it is not diagnostic since its large uncertainty also overlaps the air and Q compositions. Compared to solar wind ratios, $^{21}Ne/^{22}Ne$ in Thera-1 is lower by ~3σ and the two most precise determinations of $^{20}Ne/^{22}Ne$ are ~10σ lower (Table 1). Contemporary solar wind as a principal source of Stardust Ne is therefore ruled out, a conclusion reinforced by measured $^{3}He/^{4}He$ ratios that differ from the solar wind by >5σ (Fig. 2B). One possibility might be that the Ne composition reflects mixing of solar Ne with an air contaminant. However the source of such

a large and similar air contribution in both laboratories —comprising ~75% of the ^{20}Ne in St-1 and Thera-2 and greatly exceeding aerogel blank levels *(13)*— is not evident. Note also that ^{21}Ne/^{22}Ne consistently falls to the left of the air-solar mixing line in Fig. 2A, although this is a relatively weak constraint since the deviations are only ~1σ.

Isotopic evidence that a He component resembling Q-He is also present would go far toward establishing a Q-gas source for Stardust cometary matter. However, as discussed next, the ^{3}He/^{4}He ratios observed in St-1 and St-2 are not Q-like: their average is approximately twice the Q-He ratio. So the light noble gases in Stardust, if they have a Q-affinity, appear to be distinct from the meteoritic component in this respect. Their ^{4}He/^{20}Ne elemental ratios of ~1-20 are also distinct, much below the ~80-140 range in phase Q (Table 1).

Detection of ^{3}He, which cannot derive from terrestrial contamination, is by itself firm evidence that indigenous cometary gases are indeed present in Stardust samples. The ^{3}He/^{4}He ratio is important because in principle it can point to when comets acquired their noble gases, and from what volatile reservoir —the early protosolar nebula, a locus near the evolving Sun after the deuterium burning that elevated the level of protosolar ^{3}He, or by later implantation of solar wind radiation. Of the compositions plotted in Fig. 2B, the Jovian atmospheric ratio is thought to reflect the primordial nebular (protosolar) value, "D-burning" is an estimate of ^{3}He/^{4}He in the Sun following deuterium burning, and "Solar Wind" represents measurements of the ratio in collectors of the contemporary solar wind returned by the Genesis Mission.

The differences between the Q-He and observed ^{3}He/^{4}He ratios (Fig. 2B) cannot be attributed to excess ^{3}He produced by nuclear spallation reactions during space exposure to high-energy galactic cosmic rays (GCR). Although the abundances of ^{3}He in these samples are small (<600,000 atoms), concentrations per gram of host grains are not. The mass of grain fragments lodged in the bulbous cavity wall, assessed by Fe K_α fluorescence measurements, is ~570 nanograms/cm^2 assuming uniform areal grain density, and the average area of cavity wall material in each of the 5 analyzed samples is ~7.3 x 10^{-4} cm^2 (supporting online text). The average grain mass per sample is then ~0.42 ng, and the corresponding ^{3}He concentration, obtained by dividing this mass into the Table 1 abundances, is ~4.4 x 10^{-5} cm^3 STP/g. About half of this would have to be spallogenic to elevate ^{3}He/^{4}He from Q-He to the measured ratio (Fig. 2B). Calculations (supporting online text) show that this would require the particle to reside within the upper meter of the surface, where ^{3}He production is maximum, for times comparable

to the 4500 Ma age of the solar system. In reality, abundances of spallation products in the active surface of a comet such as Wild 2 should be essentially nil; shallow zones where they might conceivably have accumulated over long times have eroded away. Average sublimation erosion of the Wild 2 surface just since its 1974 appearance is estimated to be ~1 m *(20)*, corresponding to ~5 m in the ~20% of the surface covered by the gas and dust jets encountered by Stardust *(21)* if these source areas were active on previous apparitions.

With a degassed grain mass of ~0.42 ng, average concentrations of the principal isotopes ^{4}He and ^{20}Ne (Table 1) are ~1 and ~0.1 cm^{3} STP/g respectively. These high values have important implications for how the Stardust samples acquired their noble gases. It is clear (Fig. 3) that equilibrium solubility of nebular Ne into melt —from which the Stardust minerals are assumed to have crystallized— is many orders of magnitude too small at calculated nebular pressures to match observed Ne concentrations. A similar shortfall is seen for physical adsorption of ambient Ne in grain-surface structures, even for a favorable case, shown here, of adsorption on finely divided carbon. In contrast, Stardust Ne concentrations are interestingly comparable to those implanted in IDPs and lunar regolith grains by solar-wind ion irradiation (Fig. 3). Among known gas acquisition mechanisms, it appears that only ion implantation is capable of generating such high Ne (and He) loading in these mineral grains.

In the context of a possible Q-gas source for Stardust Ne, one sees in Fig. 3 that the Q-Ne abundances per gram of "carrier phase" in meteorites are lower than the Stardust Ne range by factors of ~10^{5}; the corresponding factors for He are ~10^{4}. However this "carrier phase", a residue isolated by chemical dissolution of silicate minerals, is itself a mixture of several mineralogic and organic components; the actual hosts of Q-gases appear to be organic materials *(22,23)*, but what their masses might be is much debated but essentially unknown *(16)*. It seems likely that the true Q-carriers comprise only a fraction of total residue mass, and thus the Fig. 3 concentrations are indicated as lower limits, possibly by orders of magnitude.

Where do we presently stand on interpreting these Ne and He distributions in Stardust material? There are two important issues. One is the nature of the material carrying the noble gases. We know from the high temperatures (≥1250°C) needed to release them that the host is refractory, consistent with the mineralogy of the grains lodged in the track wall which we have assumed to be the gas carriers. But, just on this basis, they are not the only option; organic carriers of meteoritic Q-gases also retain major fractions of their gases until heated to >1200°C

(24). Some Stardust particle tracks are rich in carbonaceous matter *(25)*, raising the possibility of an organic host. This one, however, is not. A search of bulb-wall material for organics by infrared spectroscopy was negative, setting an upper limit of ~10 femtograms on average in the samples analyzed for noble gases (supporting online text). Average ^{20}Ne concentrations would then have to exceed ~3 liters/g if the gases were trapped in organic matter; the corresponding ^{4}He loading is >20 liters/g. Trapping capacities in organic compound structures could not approach these levels. The bulb-wall grains are therefore the only plausible host material.

The second issue concerns the compositional nature of the source reservoir. Neon isotopes resemble Q-Ne, but a Q-like source for both Ne and He encounters the problems of the high ^{3}He/^{4}He and low ^{4}He/^{20}Ne ratios (Fig. 2B, Table 1). These latter ratios, however, do not necessarily reflect the elemental composition of the source reservoir. Helium thermally escapes from trapping sites more readily than Ne, so low ^{4}He/^{20}Ne could result from diffusive loss from grains during gas incorporation or over their metamorphic history. Diffusion also alters isotope ratios, with the lighter species escaping preferentially, and this led a reviewer to ask if the gases initially implanted in the grains could have been solar rather than Q-like —i.e., a direct sampling of the ancient sun, subsequently fractionated from solar ratios (Table 1) to the observed composition by extreme diffusive losses. An alternative might be gas acquisition from an initially solar reservoir that had been fractionated by mass-dependent losses to space. Both hypotheses, however, fail a central test: diffusion calculations (supporting online text) show that replication of the observed Ne and He isotope ratios requires the percentage of solar Ne depletion to greatly exceed that of the lighter He, an unphysical result either for diffusion from natural minerals or for Rayleigh distillation of a gaseous reservoir.

We conclude that the Stardust Ne data point more firmly to a Q-gas source than to other alternatives. The anomalously high ^{3}He/^{4}He and low ^{4}He/^{20}Ne ratios remain unexplained, although it may be possible to reconcile them with the Q-like Ne by invoking a two-stage model of gas acquisition and loss (supporting online text). The presence of Q-gases would be an important clue to the antiquity of the Wild 2 gas reservoir. They have just the characteristics one would expect for a fundamental constituent of the early solar nebula. They are present in all meteorites that have been subject to the experimental procedures required to isolate their carrier phase *(16)*, and ^{3}He/^{4}He in Q is close to the Jupiter atmospheric ratio (Fig. 2B), a marker for He composition in the primitive nebula.

A central question for the noble gases is where they were acquired by the comet particles. One of the surprises in samples collected from an icy object forming, and, for much of its lifetime, residing in the cold outer reaches of the solar system was the discovery that many of its constituent particles, including that in track 41, are igneous, refractory "rocklets" processed at very high temperatures, presumably close to the Sun prior to transport to the outer nebula and incorporation into Wild 2 *(1,26-28)*. Another is the finding here of high concentrations of He and Ne that, of known gas acquisition mechanisms, only ion irradiation seems capable of explaining (Fig. 3). These observations together with the isotopic data in Fig. 2 —pointing to a source containing primitive Q-Ne, and a He composition which could reflect later addition of a solar component to diffused Q-He —suggest that Stardust grains and the carbonaceous carrier now found in meteorites sampled the same Q-gas reservoir, the grains by ion implantation in an energetic environment near the young evolving Sun.

Table 1. Helium and neon abundances, relative abundances, and isotope ratios in Stardust particle track samples. *Analyzed at the University of Minnesota, USA. †Analyzed at CRPG Nancy, France. Uncertainties are ±1σ. (nm: not measured). Limits for ^{4}He and ^{3}He/^{4}He in St-3 reflect the probable presence of an anomalous ^{4}He blank contribution *(12)*. Phase Q and Solar compositions are listed for comparison. Phase Q data from *(16)*. Solar (solar wind) data are averages or ranges of measurements in Genesis collector materials *(17-19)*.

Sample	^{4}He ($\times10^{-11}$ cm^{3}STP)	^{3}He/^{4}He ($\times10^{-4}$)	^{20}Ne ($\times10^{-11}$ cm^{3}STP)	^{20}Ne/^{22}Ne	^{21}Ne/^{22}Ne ($\times10^{-2}$)	^{4}He/^{20}Ne
St-1*	7.27 ± 0.36	2.92 ± 0.26	5.34 ± 0.42	10.68 ± 0.35	2.73 ± 0.24	1.36 ± 0.13
St-2*	5.26 ± 0.30	2.47 ± 0.34	0.94 ± 0.14	9.0 ± 1.6	3.9 ± 1.1	5.60 ± 0.89
St-3*	<66.9 ± 2.4	>0.318 ± 0.032	1.06 ± 0.15	9.3 ± 1.6	4.2 ± 1.8	<63.1 ± 9.2
Thera-1†	53 ± 17	nm	2.47 ± 0.65	12.9 ± 3.2	2.45 ± 0.29	21.4 ± 4.9
Thera-2†	17.5 ± 3.8	nm	5.80 ± 0.43	10.49 ± 0.24	2.79 ± 0.17	3.0 ± 1.3
Phase Q		1.45 ± 0.15		10.1 – 10.7	2.78 – 2.94	110 ± 30
Solar		4.44 ± 0.10		13.90 ± 0.08	3.35 ± 0.07	520 - 670

References and Notes

1. D. Brownlee *et al.*, *Science* **314**, 1711 (2006).
2. S. Messenger, *Meteorit. Planet. Sci.* **37**, 1491 (2002).
3. A. O. Nier, D. J. Schlutter, *Meteoritics* **28**, 675 (1993).
4. K. Kehm *et al.*, *30th Lunar Planet. Sci. Conf.* abstract 1398: CD-ROM (1999); available online at http://www.lpi.usra.edu/publications/absearch.
5. R. O. Pepin, R. L. Palma, D. J. Schlutter, *Meteorit. Planet. Sci.* **36**, 1515 (2001).
6. R. L. Palma, R. O. Pepin, D. J. Schlutter, *Meteorit. Planet. Sci.* **40**, A120 (2005).
7. D. J. Joswiak, D. E. Brownlee, R. O. Pepin, D. J. Schlutter, in *Dust in Planetary Systems,* H. Krüger, A. Graps, Eds. (ESA Publication SP-643, 2007), pp. 141-144.
8. K. Lodders, R. Osborne, *Space Sci. Rev.* **90**, 289 (1999).
9. M. Gounelle, P. Spurny, P. A. Bland, *Meteorit. Planet. Sci.* **41**, 135 (2006).
10. T. Owen, A. Bar-Nun, I. Kleinfeld, *Nature* **358**, 43 (1992).
11. N. Dauphas, *Icarus* **165**, 326 (2003).
12. R. O. Pepin, *Earth Planet. Sci. Lett.* **252**, 1 (2006).
13. A brief report of experimental methods and noble gas data obtained at CRPG Nancy (Table 1) appeared earlier in *(27)*.
14. Materials and methods are available as supporting material on Science Online.
15. J. E. Shelby, *Phys. Rev. B* **4**, 2681 (1971).
16. H. Busemann, H. Baur, R. Wieler, *Meteorit. Planet. Sci.* **35**, 949 (2000).
17. J. C. Mabry *et al.*, *38th Lunar Planet. Sci. Conf.* abstract 2412: CD-ROM (2007); available online at http://www.lpi.usra.edu/publications/absearch.
18. V. S. Heber *et al.*, *38th Lunar Planet. Sci. Conf.* abstract 1894: CD-ROM (2007); available online at http://www.lpi.usra.edu/publications/absearch.
19. A. Grimberg, D. S. Burnett, P. Bochsler, H. Baur, R. Wieler, *Space Sci. Rev.* **130**, 293 (2007).
20. D. E. Brownlee *et al.*, *Science* **304**, 1764 (2004).
21. Z. Sekanina, D. E. Brownlee, T. E. Economou, A. J. Tuzzolino, S. F. Green, *Science* **304**, 1769 (2004).
22. U. Ott, R. Mack, S. Chang, *Geochim. Cosmochim. Acta* **45**, 1751 (1981).

23. Y. Marrocchi, S. Derenne, B. Marty, F. Robert, *Earth Planet. Sci. Lett.* **236**, 569 (2005).
24. G. R. Huss, R. S. Lewis, S. Hemkin, *Geochim. Cosmochim. Acta* **60**, 3311 (1996).
25. S. A. Sandford *et al., Science* **314**, 1720 (2006).
26. D. E. Brownlee, D. Joswiak, J. Bradley, G. Matrajt, *38th Lunar Planet. Sci. Conf.* abstract 2189: CD-ROM (2007); available online at http://www.lpi.usra.edu/publications/absearch.
27. K. D. McKeegan *et al.*, *Science* **314**, 1724 (2006).
28. M. E. Zolensky *et al.*, *Science* **314**, 1735 (2006).
29. P. R. Mahaffy, T. M. Donahue, S. K. Atreya, T. C. Owen, H. B. Niemann, *Space Sci. Rev.* **84**, 251 (1998).
30. J. Geiss *et al.*, *Space Sci. Rev.* **110**, 307 (2004).
31. R. O. Pepin, R. L. Palma, D. J. Schlutter, *Meteorit. Planet. Sci.* **35**, 495 (2000).
32. P. Eberhardt *et al.*, in *Proc. 3rd Lunar Sci. Conf., Vol. 2*, D. Heymann, Ed. (MIT Press, Cambridge MA, 1972), pp. 1821-1856.
33. J. F. Wacker, *Geochim. Cosmochim. Acta* **53**, 1421 (1989).
34. A. Jambon, H. Weber, O. Braun, *Geochim. Cosmochim. Acta* **50**, 401 (1986).
35. J. Matsuda *et al.*, *Science* **259**, 788 (1993).
36. J. A. Wood, G. E. Morfill, in *Meteorites and the Early Solar System*, J. F. Kerridge, M. S. Matthews, Eds. (Univ. of Arizona Press, Tucson, 1988), pp. 329-347.
37. E. Anders, N. Grevesse, *Geochim. Cosmochim. Acta* **53**, 197 (1989).
38. This study was funded at Nancy by the Centre de Recherches Pétrographiques et Géochimiques (CNRS) and the Centre National d'Etudes Spatiales (CNES), and at Minnesota by Grant NAG5-11732 from the NASA Cosmochemistry Program. Part of this work was performed under the auspices of the U.S. Department of Energy by Lawrence Livermore National Laboratory under Contract DE-AC52-07NA27344. We thank Michael C. Martin (Advanced Light Source, Lawrence Berkeley National Laboratory) for helpful discussions. Zack Gainsforth (U.C. Berkeley, Space Science Laboratory), and Matthew Marcus and Sirine Fakra (ALS, LBNL), provided crucial support for the XANES analyses. Encouragement from the Stardust Preliminary Examination Team, in particular from K. McKeegan and D.E. Brownlee, is gratefully acknowledged. This is CRPG contribution 1870.

Supporting Online Material
www.sciencemag.org
Materials
Methods
Figs. S1 to S3
SOM Text
Table S1
References

Figure Captions

Fig. 1. **(A)** Track #41, aerogel cell C2044. Following entry into the aerogel at ~6 km/s (top) the particle was subject to intense frictional heating and fragmented, creating a prominent bulbous cavity (middle) walled with melted aerogel silica and small grain fragments. Samples analyzed in this study were taken from the cavity wall; the triangular quarry left by the sampling tool is visible at the upper left. Two larger pieces (~10 and 15 μm) of the original particle survived to penetrate more deeply, along trajectories marked by the narrow individual tracks (bottom). Track length is ~10 mm from entry to deepest track terminus. **(B)** Example of an extracted sample: Thera-1, analyzed at CRPG Nancy. Most of the area is undisturbed aerogel. The dark band (lower left) is the snippet of compressed cavity wall material excised along the track by the sampling tool. Other samples in this study are pictured in *(13)*.

Fig. 2. **(A)** Neon isotope ratios in Ne-Q, and in Stardust samples St-1 and Thera-2 (Table 1). Ne-Q isotopic range (shaded area) from *(16)*. The solid line extending from Air-Ne defines compositions generated by mixtures of air with solar wind Ne, offscale at $^{20}Ne/^{22}Ne$ = 13.90 ± 0.08, $^{21}Ne/^{22}Ne$ = 0.0335 ± 0.0007. **(B)** Helium isotope ratios in St-1 and St-2 (Table 1), compared to $^{3}He/^{4}He$ measured in other solar-system reservoirs: 1.45 ± 0.15 x 10^{-4} in He-Q *(16)*, 1.66 ± 0.05 x 10^{-4} in Jupiter's atmosphere *(29)*, 4.44 ± 0.10 x 10^{-4} in Genesis measurements of present-day solar wind *(17-19)*. The ratio in the Sun following deuterium burning is estimated to be 3.65 ± 0.38 x 10^{-4} *(30)*. Errors in (A) and (B) are 1σ.

Fig. 3. Concentration ranges of ^{20}Ne in cm^3 STP/g (1 cm^3 STP = 2.69 x 10^{19} atoms) in the Stardust samples, the Q-Ne carrier phase *(16)*, ~5-10μm IDPs *(31)* and ~1-10μm lunar regolith grains *(32)* irradiated by the solar wind; measured in the laboratory for adsorption on carbon black at ~20-400°C *(33)*; and calculated for Ne dissolved in basaltic melt and partitioned into Fe crystals (there are no available data for FeS partitioning), using gas-melt distribution and iron-melt partition coefficients from *(34)* and *(35)*. Stardust concentrations from measured ^{20}Ne abundances (Table 1) and average host grain masses of 0.42 ng per sample. The plotted IDP range is for the Group 2 IDPs in *(31)*, which have an average He isotope ratio consistent with implanted solar wind. Concentrations of adsorbed and dissolved Ne depend on Ne partial pressure in the ambient gas. Plotted ranges assume a total nebular pressure of 10^{-3} atmospheres (100 Pa) close to the Sun *(36)*, and a corresponding Ne partial pressure of 10^{-7} atm *(37)*. The highest concentration of dissolved Ne, at ~10^{-11} cm^3 STP/g, is for equilibrium solution into basaltic melt *(34)*; the arrow points to concentrations partitioned into iron crystals, lower by a factor of ~10 at low pressure *(35)*. Error bars on the Stardust range reflect a conservative estimate of a factor 3 uncertainty in calculations of concentrations.

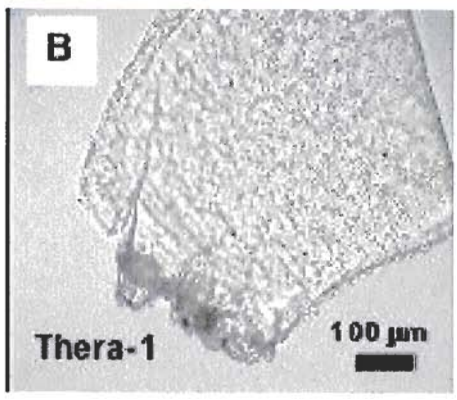

Fig. 1

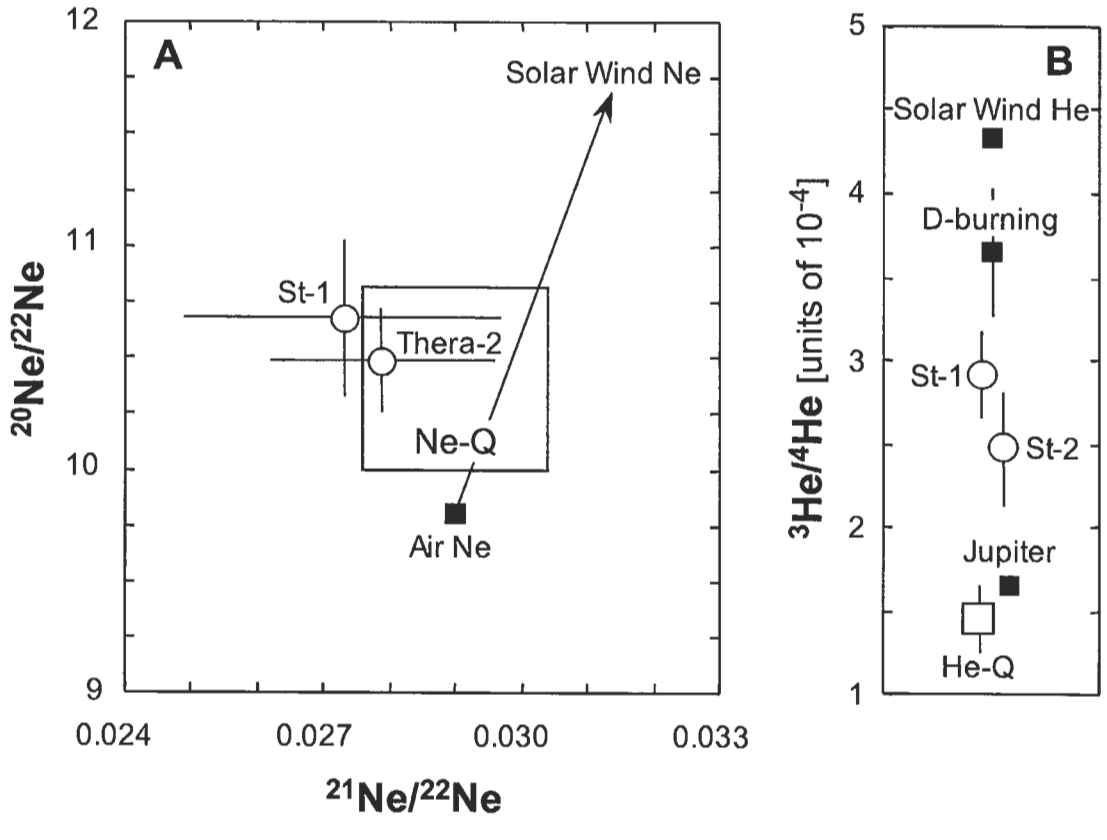
A
B
Solar Wind Ne
St-1
Thera-2
Ne-Q
Air Ne
Solar Wind He
D-burning
St-1
St-2
Jupiter
He-Q
$^{20}Ne/^{22}Ne$
$^{21}Ne/^{22}Ne$
$^{3}He/^{4}He$ [units of 10^{-4}]
12
11
10
9
0.024
0.027
0.030
0.033
5
4
3
2
1

Fig. 2

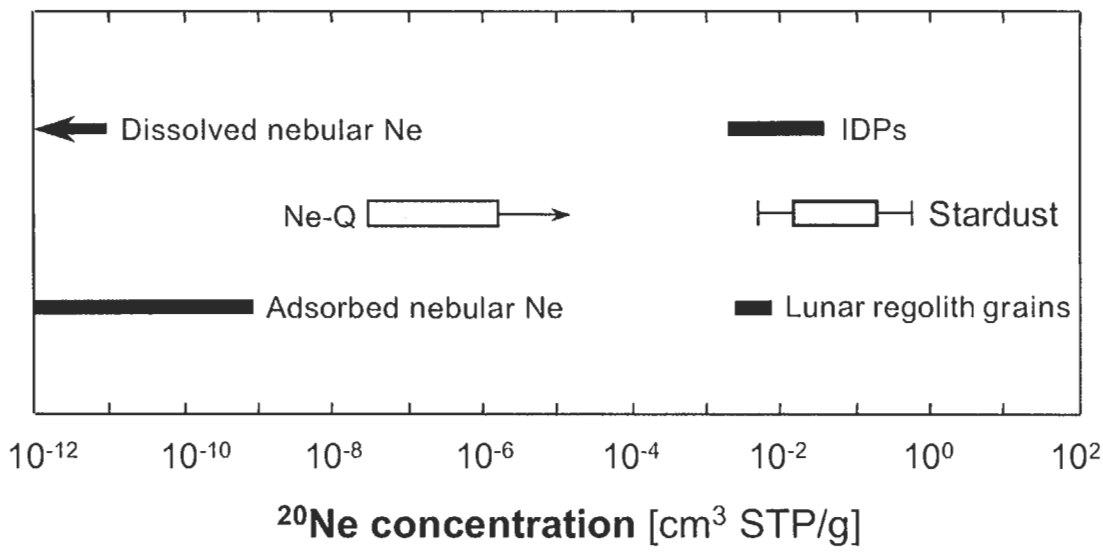
Dissolved nebular Ne
IDPs
Ne-Q
Stardust
Adsorbed nebular Ne
Lunar regolith grains
10-12
10-10
10-8
10-6
10-4
10-2
100
102
20Ne concentration [cm3 STP/g]

Fig. 3

Supporting Online Material

Materials

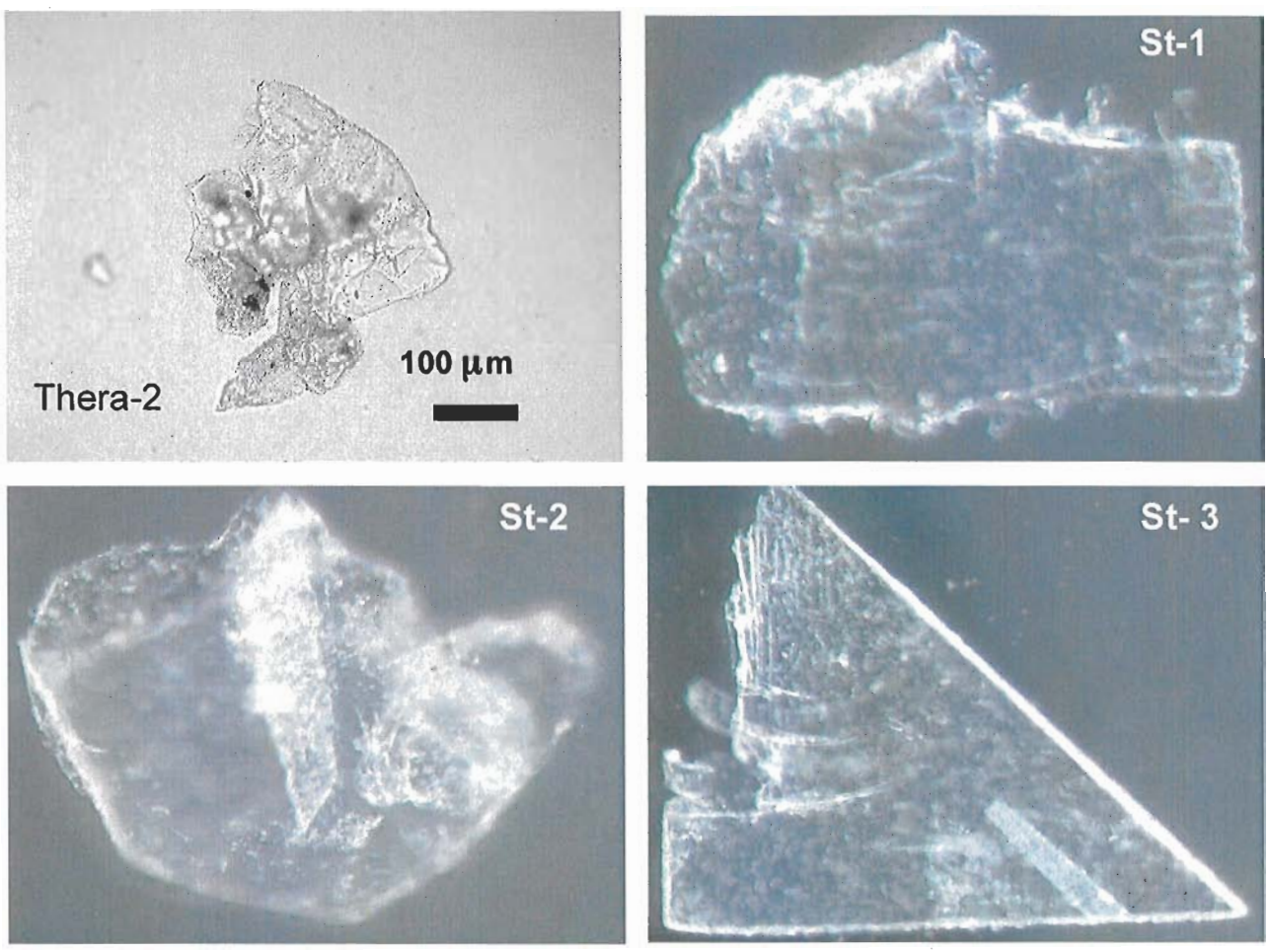

Fig. S1. Stardust samples Thera-2 (CRPG Nancy) and St-1, St-2, St-3 (University of Minnesota) extracted from the bulbous cavity wall of track #41, aerogel cell C2044. Thera-1 is shown in Fig. 1B, main text. Actual cavity-wall materials occupy only small areas of the pictured aerogel tiles. The Minnesota samples are ~1mm in largest dimension.

Methods

1) CRPG Nancy

Stardust samples were provided by the Isotope Preliminary Examination Team (PET) led by K. McKeegan *(S1)*. We received blank aerogel chips, flown aerogel chips and two fragments of bulbous aerogel. The first piece was extracted as an aerogel "keystone" (*S2*) from the wall of a large bulbous track (track #41, cell C2044). This sample will be referred to in the following as Thera-1 (Fig. 1B, main text). This sample, together with blank and flown samples, were analyzed

after extensive blank determination (see below). Given the results of the first allocation, a second allocated larger piece of the same wall (Thera-2) was analyzed together with another piece of flown aerogel (Fig. S1).

Aerogel fragments were handled in a clean room (class 10,000 in the room, class 100 in extraction boxes) under a microscope using a clean single-hair paintbrush attached to a manipulator. It was not possible to weigh aerogel chips due to their small size, and we have estimated optically the surface area of the chips. Assuming that all chips have a comparable thickness, the surface area of a sample gives a first order idea of the aerogel sample quantity. Samples were loaded in pits of a laser cell in operation at CRPG Nancy, which was connected to a high vacuum line and baked at 80°C (Thera-1 run) and 100°C (Thera-2 run) overnight. The samples were then left under vacuum (1.5×10^{-9} mbar) at room temperature for 3 weeks (Thera-1) and 1 week (Thera-2), respectively.

Samples were heated using a CO_2 infrared (λ = 10.6 μm) laser mounted on an x-y stage and monitored through a microscope equipped with a CCD camera. We used a visible (He-Ne) laser to point samples and discovered that even the weak pointer laser provoked vibrations of the fragments under illumination. Hence we heated the chips with great care by very slowly increasing the power of the CO_2 laser in order to avoid samples jumping out of the pits. We lost one blank aerogel sample and did not analyze other small blank aerogel samples. Fortunately, the flown aerogel chips and the bulbous chips were bigger and could be safely analyzed. Once thermal coupling of the aerogel sample with the laser beam was achieved, aerogel chips could be totally melted.

Extracted gases were handled in a new facility at CRPG developed for the analysis of very low amounts of noble gases and nitrogen implanted in Genesis target material. Gases were cleaned up with two Ti sponge getters (one at 650°C, the other at room temperature), and analyzed in two fractions, He plus Ne, and Ar, with a VG5400 Micromass@ static mass spectrometer *(S3)*. The blanks were thoroughly investigated and analyses started only when the blanks were indistinguishable from those of the purification line alone, as determined during several months prior to these experiments. Blanks measured without the laser on, and with the laser illuminating a metal surface adjacent to the samples, were indistinguishable. The blank values (n = 6) were $1.1 \pm 0.6 \times 10^{-10}$, $1.9 \pm 0.4 \times 10^{-11}$, and $2.4 \pm 0.7 \times 10^{-12}$ cm^3 STP for ^{4}He, ^{20}Ne, and ^{36}Ar respectively. The amounts of argon released during sample runs were indistinguishable from those of the blank runs.

In all cases, blank corrections were critical. Potential sources of blank are (i) instrumental blank, determined without heating a sample, and (ii) the aerogel. The former should be approximately constant over a given period, whereas the latter should be proportional to the size of the aerogel sample. Fig. S2 represents the amount of He and Ne during the various runs as a function of the aerogel surface area for each sample. If (ii) was dominant, one would expect a correlation. On the contrary, if most of the blank is instrumental, there should not be any relationship between the aerogel chip size and the blank. Extractions of flown aerogel without bubbles are comparable to the blanks (represented by the shaded area in Fig. S2), given uncertainties. This suggests strongly that the instrumental blank dominates over the aerogel blank for the sample sizes we analyzed.

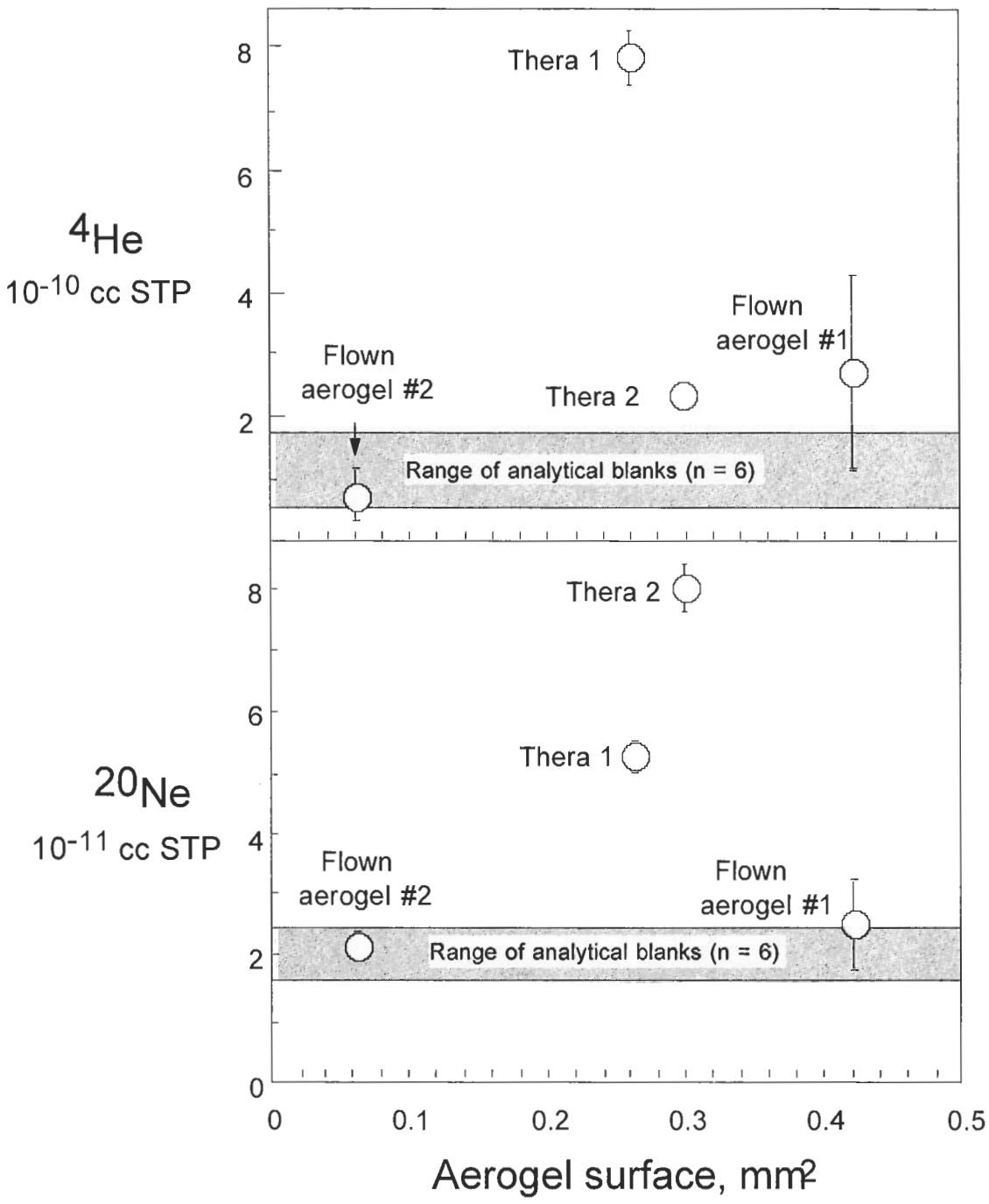

Fig. S2. He and Ne amounts extracted from aerogel chips of variable sizes (CRPG Nancy). The shaded areas represent the range of blank values for the analytical facility. There is no correlation between the amounts of He and Ne and the aerogel sample surface, strongly suggesting that the main source of blank is not the aerogel itself. Flown aerogel has He and Ne blanks undistinguishable from the procedural one. "Thera" samples have He and Ne contents clearly above the system blanks.

2) University of Minnesota

Three different sample types were analyzed: **(i)** A ~1.5 mm^2 sample cut from a block of Stardust flight spare aerogel (E226-5B) supplied by M. Zolensky (Astromaterials Research and Exploration Science, NASA-Johnson Space Center) to determine the feasibility of measuring noble gases in particles embedded in aerogel. **(ii)** A blank sample ~1.5 mm^2 in area (keystone CO44) of Stardust flight aerogel excised from an aerogel cell containing no visible cometary material, provided by the PET for further aerogel blank measurements. **(iii)** Three samples of aerogel-embedded cometary material (Fig. S1) extracted *(S2)* from the same bulbous track wall (track #41, cell C2044) distributed to the CRPG Nancy group, allocated to Minnesota by the PET to enable independent measurements in two laboratories. These samples are designated St-1, St-2, and St-3.

Samples were wrapped in Pt foil packets and attached across electric power leads in a miniature vacuum furnace. Following a 150-200 °C bakeout (all samples except St-3; see below), gases were extracted by stepped heating to ~1075°C at computer controlled power levels, with 15 or 20 second dwell times at each temperature, in a technique similar to that used for lunar grains *(S4)* and IDPs *(S5)*. Gas release temperatures were repeatedly monitored by optical pyrometer, with an uncertainty of ± 50°C. Except for temperatures above ~1075°C, there were only minor modifications of the computer controlled pulse heating procedures described in *(S4)*.Three initial sequential heating steps at increasing power heated the samples to ~250°C. Although the gases liberated in these steps were analyzed isotopically, the heating served primarily as a clean-up procedure to remove any surface sited or adsorbed gases not removed during the bakeout. Helium and Ne released in these steps was at or below the system blank levels described below. Up to 10 sequential heating steps at increasing power were then applied, resulting in step degassing temperatures ranging from ~250 to ~1075°C. Cumulative release of ^{4}He and ^{20}Ne was monitored during the degassing. No He or Ne signals above blank levels were seen up to the maximum temperature (~1075°C) reached by the computer controlled system (Fig. S3). An external power supply was subsequently used to manually increase the temperature above 1075°C while monitoring the Pt packet temperature with an optical pyrometer. St-1 began to degas above blank levels at ~1250°C, and St-2 and St-3 at ~1300°C. Heating was terminated for all samples at ~1400°C, the maximum attainable temperature for the Stardust Pt foil packets.

The loading and bakeout of St-3 were handled slightly differently than for St-1 and St-2. Because of the possibility that the samples might contain a gas component released at low temperatures that would have been lost from St-1 and St-2 during bakeout, there was no bakeout following the loading of St-3 into the gas extraction system. Despite this, the He and Ne signals observed during the low temperature (<250 °C) and computer controlled heatings up to ~1075°C were still indistinguishable from blank values.

Earlier studies of flight spare aerogel with a residual gas analyzer had revealed large background abundances of H, H_2O, CO and CO_2, so evolved gases were continually purified by a room temperature Westinghouse@/WL getter and cryopumped at LN_2 temperature. No attempt was made to measure Ar, whose abundance was anticipated to be undetectable above background. Helium and Ne were analyzed statically in a 3.75" double focusing Mattauch-Herzog geometry mass spectrometer equipped with pulse counting detectors, an instrument specifically designed for high sensitivity analyses of trace amounts of noble gases *(S6)*. The mass spectrometer was

cryopumped at LN_2 temperature during all analyses. Signals at masses 18 ($H_2{}^{16}O$), 40 (^{40}Ar), and 44 ($^{12}C^{16}O_2$), measured along with the Ne isotopes, were very low. Additionally, Ne was analyzed at an ionizing energy of 35eV, experimentally determined to be low enough that doubly ionized ^{40}Ar and CO_2 were undetectable at Ne masses 20 and 22. As a result, corrections to the Ne isotopic values consisted only of the $H_2{}^{18}O^+$ correction to mass 20. These ranged from 3.7% of the mass 20 abundance for the sample with most Ne (St-1) to 13-19% for St-2 and St-3.

Sensitivities for He and Ne were derived from repeated analyses of air samples metered into the system from calibration cans designed to permit accurate volumetric splitting, with non-noble gases removed by gettering and freezing out on charcoal at LN_2 temperature. Detection limits for the mass spectrometer used in this study were approximately 1×10^{-14}, 6×10^{-13}, and 2×10^{-13} cm^3 STP for ^3He, ^4He, and ^{20}Ne, respectively.

Accurate measurements of blank levels were critical for the Stardust analyses. Aerogel volatiles may be separated into gas from the Stardust grains, and gas from all other sources. Gases intrinsic to aerogel itself may lie on surfaces and/or be trapped within the aerogel. To examine possible intrinsic noble gas sources, a ~1.5 mm^2 sample [(i) above] from flight spare block E226-5B was heated in nine 15 s steps from 300 to 1330°C and then reheated using the same procedures. Reheated values determined the system blank. All reported blank abundances are cumulative over the given temperature ranges. In the initial heating, the ^4He abundance was 3.4×10^{-11} cm^3 STP below 1000°C, increasing at 1330°C to 6.9×10^{-11} cm^3 STP. In the reheat, the ^4He abundance was 5.1×10^{-11} cm^3 STP, whereas ^3He and ^{20}Ne were indistinguishable in the initial and reheat runs (at $\sim 1.3 \times 10^{-14}$ and $\sim 6.6 \times 10^{-12}$ cm^3 STP, respectively). These data suggested that a small intrinsic ^4He component might be present in the aerogel, but show no evidence for intrinsic ^3He or ^{20}Ne.

Blank analyses were repeated for the flight aerogel keystone C044 [(ii) above]. It was initially heated to 200°C for 20 s to release contamination loosely trapped in the sample or sample holder, then heated in three 15 s steps at 1140, 1250, and 1330 °C, with cumulative gas measurements taken after the final heating step. ^3He, ^4He and ^{20}Ne abundances were indistinguishable between cold blanks (no heating), the 200°C heating, the 1330°C initial heating, and a 1330°C reheating (system blank) at approximately 1.2×10^{-14}, 1.4×10^{-11}, and 2.4×10^{-12} cm^3 STP, respectively. Thus, as observed earlier in the flight spare aerogel, there was no evidence for any ^3He or ^{20}Ne intrinsic to the aerogel above system blank values. Moreover, in contrast to the flight spare aerogel, the Stardust flight aerogel yielded no detectable intrinsic ^4He, and overall system blanks were lower.

Blanks, both cold and hot, were run on empty Pt foils. Duplicate reheats were also done on every sample. Since the clearest indication of non-terrestrial helium was the presence of an unambiguous ^3He signal, utmost care was taken to evaluate the ^3He blank value accurately. Seventeen ^3He blank determinations were made throughout the sample analysis period. The values obtained were extremely consistent [$(1.20 \pm 0.08) \times 10^{-14}$ cm^3 STP] and did not depend on the heating conditions of the run—time, temperature, or number of steps—but were instead dominated by counting statistics. This blank contributed 35% (St-1 and St-3) to 48% (St-2) of the ^3He liberated during the high temperature sample analyses (Fig. S3).

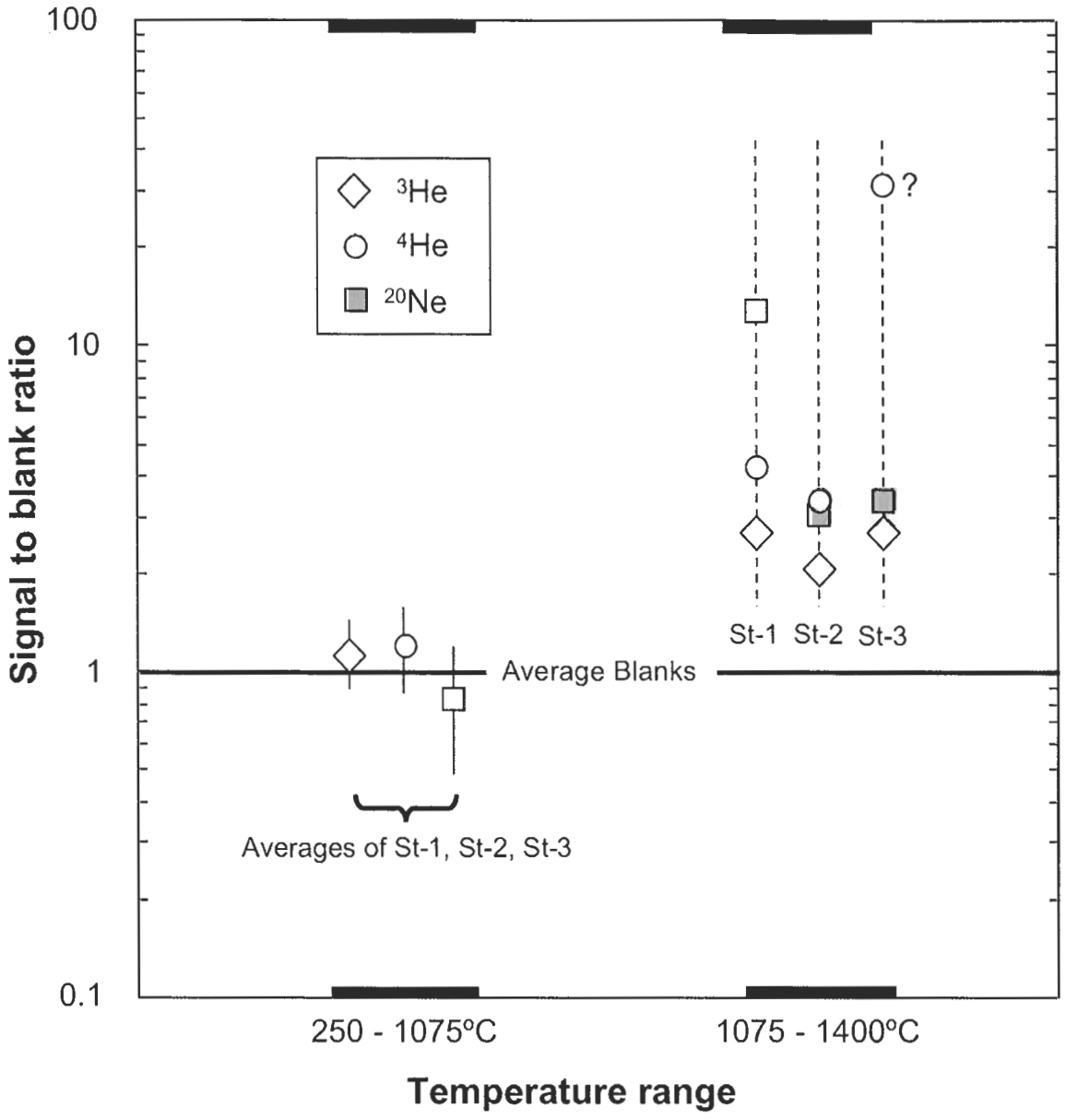

Fig. S3. Signal to blank ratios for cumulative releases of ^{3}He, ^{4}He, and ^{20}Ne from samples St-1, St-2, and St-3 (Minnesota) during step-heating from 250°C to 1075°C, and from 1075°C to 1400°C. Sample abundances evolved over the lower temperature range are indistinguishable from cumulative blank levels over the same range. High temperature gas release above blank levels commenced at ~1250 °C for St-1, and at ~1300 °C for St-2 and St-3. Errors on sample abundances include measurement uncertainties and, for the lower temperature data, scatter around the averages of the three samples. All errors are s.e.m. They are smaller than the symbol sizes for the high-temperature data. The high-temperature ^{4}He abundance in St-3 is questionable because of a suspected high blank. Average cumulative blank abundances in Fig. 3, in cm^{3} STP, are $1.20 \pm 0.08 \times 10^{-14}$, $1.4 \pm 0.5 \times 10^{-11}$, and $2.4 \pm 0.6 \times 10^{-12}$ for ^{3}He, ^{4}He, and ^{20}Ne respectively over the 250-1075°C heating range, and $1.20 \pm 0.08 \times 10^{-14}$, $2.2 \pm 0.4 \times 10^{-11}$, and $4.4 \pm 1.2 \times 10^{-12}$ over the 1075-1400°C range.

As a result of their dependence on the heating conditions of the run, and thus having fewer overall blank measurements, ^{4}He and Ne blank corrections have greater associated error than those for ^{3}He. Only high temperature heatings similar to those releasing sample gas were used in determining the ^{4}He and Ne blanks, since in those instances a greater blank was consistently observed. In the case of ^{4}He, the average blank abundance of $(2.17 \pm 0.36) \times 10^{-11}$ cm^3 STP represented 23% (St-1), 29% (St-2), and 3% (St-3) of the ^{4}He liberated during the high temperature sample analyses, whereas for ^{20}Ne, the average blank of $(4.4 \pm 1.2) \times 10^{-12}$ cm^3 STP represented 8% (St-1), 32% (St-2) and 29% (St-3) of the ^{20}Ne released (Fig. S3).

The reheat ^{4}He blank level for sample St-3 was anomalously high, ~4 times the average given above for all other ^{4}He blanks. The gas released in the reheat was probably not from the sample since the ^{3}He value equalled the blank. The high ^{4}He gas abundance (and correspondingly low ^{3}He/^{4}He value compared to St-1 and St-2) observed in St-3 is therefore most likely due to evolution of extraneous ^{4}He from a sample holder assembly for St-3 which had not been completely degassed of contaminant air He prior to loading. It was released only at the highest temperatures, since the sample was heated to ~1075°C earlier with no liberated gas observed above blank. Suspicion about the validity of the measured ^{4}He abundance in St-3 is reflected in Table 1 (main text), where the ^{4}He gas abundance and ^{4}He/^{20}Ne ratio are listed as upper limits, and the ^{3}He/^{4}He as a lower limit. The ^{3}He abundance of 2.13×10^{-14} cm^3 STP, however, is comparable to those in St-1 and St-2 (2.12×10^{-14} and 1.30×10^{-14} cm^3 STP respectively).

Supporting Text

1) Bulb-wall Mineralogy and Grain Masses: Space Sciences Laboratory, University of California Berkeley

We analyzed captured cometary material in track 41 using synchrotron-based microbeam X-ray Fluorescence and X-ray Near-Edge Absorption Spectroscopy (XANES), utilizing the μXANES beamline 10.3.2 at the Advanced Light Source, Lawrence Berkeley Laboratory. The synchrotron x-ray beam was focused to a beamspot several microns in diameter by Kirkpatrick-Baez mirrors, and tuned in energy using an upstream monochrometer. The energy width of the monochromatic beam was ~1 eV. The track was extracted from its aerogel tile using the "keystoning" technique *(S2).* The block of aerogel, measuring 4.5mm x 9.5 mm x 11 mm, completely contained the track and terminal particles. To determine the mineralogy of the Fe-bearing phases, 33 grains or grain clusters in the track bulb wall were analyzed using Fe XANES. Here we scanned in energy across the K-edge of Fe, and fit the normalized spectrum using non-negative linear least squares to a reference library consisting of 83 reference spectra from 54 different minerals in 24 different mineral groups (metal, sulfide, carbide, olivine, orthopyroxene, clinopyroxene, glass, and others). While there can be strong degeneracies between individual minerals within groups, identification of mineral families is generally reliable. This assay yielded the following average distribution of total Fe, in atom%, among identified mineral constituents in the bulb wall: 9% in metal, 51% in sulfides, 24% in carbides, and 16% in silicates, glasses, and other (unidentified) constituents. The corresponding mass distributions are 6 wt.% metal (with metal taken to be Fe), 53 wt.% sulfides (as FeS), 17 wt.% carbides (as Fe_3C), and 24 wt.% silicates + other (with an

atom% composition assumed to be the CI composition listed in Table 1 of *(S7)*). The two large particles (~10-15 μm) lodged at track termini (Fig. 1A, bottom) are FeNi (kamacite). The incident Stardust particle was clearly rich in iron and iron-sulphur compounds such as troilite and pyrrhotite.

The mass of Fe in the track bulb was estimated by comparing background-subtracted Fe K_α fluorescence to that of a scan of the NIST 1833 standard film using identical parameters (11 keV beam energy, 100ms dwelltime per pixel, 5μm x 5μm pixel size). Corrections were made for attenuation of the fluorescence photons due to absorption in the aerogel block containing the track. The measurements gave an Fe mass of 43 ng in a projected bulb-wall area of 3.6×10^{-2} cm^2. Multiplication by π converted the projected area to the actual bulb-wall area (assumed approximately cylindrical) of 0.113 cm^2, resulting in an average areal Fe density of 380 ng/cm^2. The mineral speciation given above for Fe yielded elemental masses/cm^2 of S (111 ng), C (7 ng), O (43 ng), Mg (14 ng), and Si (18 ng), for a total bulb-wall grain mass of ~570 ng/cm^2. The average area of bulb-wall material in each of the 5 samples analyzed for noble gases was calculated in two ways: (a) from the area of bulb wall material contained in each sample, estimated from the sample images in Figs. 1B and S1; and (b) from the total wall area contained in the excised keystone —assumed to be equally partitioned into the 5 samples— obtained by direct measurements on the keystone quarry seen in Fig. 1A. The two calculations agreed to ± ~10% and gave an average of $\sim 7.3 \times 10^{-4}$ cm^2 per sample. The average grain mass per sample is then ~0.42 ng.

2) Bulb-wall Organics: Lawrence Livermore National Laboratory

Measurements of organic components in an aerogel sample of the track 41 bulb wall, cut under an angle to the particle track, were obtained with Fourier transform infrared (FTIR) microscopy at the Advanced Light Source (ALS), Lawrence Berkeley National Laboratory. The non-invasive nature of IR spectroscopy and high sensitivity to chemical functional groups makes this an ideal technique for fingerprinting. A typical measurement records a spectrum of IR absorbance in the sample as a function of the wavelength. The basic principle is that the IR light is being absorbed only if the frequency matches exactly the frequency of the vibrational mode of a chemical functional group and the vibration causes an asymmetric change in the charge distribution within the molecule (dipole moment). Atoms of a molecule vibrate with characteristic frequencies (normal modes) governed by their chemical bonds and symmetry environment. Vibrational mode sets are unique for every molecular configuration. FTIR measurements have successfully detected organic compounds in thin TEM sections of Stardust particles *(S8, S9)* and by mapping of whole keystones with particle tracks.

Although the FTIR microscope is attached to the synchrotron source, an internal source was used for these particular measurements. With a small aperture, this source has a good signal-to-noise ratio with ~40 μm lateral resolution. The SpectraTech Nic-Plan IR microscope at the ALS beamline is equipped with a ThermoNicolet Magna 760 FTIR bench. A KBr beamsplitter was placed in the beam path and the transmitted light was collected with a MCT-A detector between 650 and 4000 cm^{-1} with 4 cm^{-1} spectral resolution. Spectra were normalized to the spectrum of the beam through the air and typical collection times were between 12 and 256 seconds per

point. A < 200 μm thick slice of aerogel cut across the particle track was mounted between two metallic foils with a small hole. IR analyses were carried out both in the track wall and, for blank corrections, hundreds of microns away from the track wall. The sample was placed on a sub-micron precision microscope stage and measured in air after the optical and infrared beams were co-aligned.

Measured blank-corrected areal densities of the $-CH_2$. $-CH_3$, and C=O functional groups in the bulb wall, in number/cm^2, were <9.1 x 10^{10}, 1.6 x 10^{11}, and <1.4 x 10^{11} respectively. The corresponding hydrocarbon mass, calculated from the measured densities and the molecular weights of the functional groups, is <13 pg/cm^2. Multiplication by the average area of bulb-wall material in each of the 5 samples, estimated above to be ~7.3 x 10^{-4} cm^2, yields an average organic abundance per sample of <10 fg. Lower limits on ^{20}Ne and ^{4}He concentrations, from this mass and average gas abundances per sample from Table 1 (main text), would then range from >3 liters/g to >20 liters/g respectively if the gases were hosted in organic matter; implied minimum densities of trapped noble gas atoms in the material, in number per functional group, are ~3 for ^{20}Ne and ~20 for ^{4}He. Trapping at such levels is clearly implausible, and would remain so even if the masses of functional groups not included in the FTIR survey (e.g., C-N, C=C) exceeded the measured upper limit by an unlikely order of magnitude.

3) Spallation Production of ^{3}He and ^{21}Ne

Production rates of ^{3}He and ^{21}Ne by GCR-induced spallation reactions are maximum in the upper meter or so of an irradiated body, and fall off rapidly with increasing depth. Particles exposed to GCR radiation at these near-surface locations thus require minimum residence times in order to accumulate a given inventory of spallogenic nuclides. Applied to Wild 2, the GCR production rate of ^{3}He in a particle with the composition given above is ~5.6 x 10^{-9} cm^3 STP/g per Ma if residing on the surface, and ~3.3 x 10^{-9} cm^3 STP/g per Ma if buried to a depth of 1 m in cometary ices. Production rates were calculated from element-specific spallation yields as functions of depth in a large body *(S10)*, where S yields were interpolated between those for Si and Fe since S is not included among the target elements tabulated in *(S10)*. With an average ^{3}He loading of ~4.4 x 10^{-5} cm^3 STP/g in the cavity-wall samples (main text), a GCR exposure time of ~3900 Ma at zero depth or ~6600 Ma at 1 m would be needed to generate half the observed ^{3}He and thus elevate ^{3}He/^{4}He from the Q-He ratio to its measured values. A similar calculation using ^{21}Ne production rates *(S11)* yields a spallogenic contribution of <1% of the measured ^{21}Ne at either location.

4) Diffusion Calculations and Gas Acquisition Modelling

In response to a suggestion by a reviewer that our observed He and Ne isotopic and elemental ratios might have been derived from a solar composition reservoir by fractionation during a loss process, we have calculated the isotopic fractionations that would result for He and Ne due to Fick's Law diffusion from a spherical particle (for a range of radii between 1 and 75 μm) of a component with a uniform initial distribution in the grain (as would result from trapping from a gas reservoir during grain formation), and of a component present in a thin shell of a few

hundred Å depth on the surface of such spherical grains (as would result from a solar wind-like ion irradiation). We also calculated the fractionations that would be generated by Rayleigh distillation of He and Ne from a well-mixed gaseous reservoir, prior to the possible incorporation of such gases into a Stardust particle, and allowing for possible gas diffusion rate-relationships for isotopic pairs other than square root of mass —i.e., gas loss processes more complicated than simple diffusion into a vacuum.

In all of these cases the fractional losses required to fractionate the $^{3}He/^{4}He$ and $^{20}Ne/^{22}Ne$ ratios from solar to the observed ratios were larger for ^{22}Ne than for ^{4}He, usually by about an order of magnitude. This cannot happen in a Rayleigh distillation, where fractional escape decreases with increasing mass. If such fractionations occurred in diffusive losses from a solid grain, they would require that the diffusion coefficient for He in the grain was much less than that for Ne, and we would expect to measure a $^{4}He/^{22}Ne$ ratio above the solar value. Since the observed $^{4}He/^{20}Ne$ ratio is fractionated from the solar ratio by about two orders of magnitude in the opposite direction to the calculation, and since diffusion coefficients in natural solids are expected to be greater for He than for Ne, we conclude that the measured isotopic and elemental ratios could not have been derived from a solar composition precursor by normal physical processes.

Although for these reasons it does not appear possible to derive Stardust compositions directly from an initially solar-like reservoir, an alternative two-stage scenario of gas acquisition and diffusive fractionation, which does call for the presence of a component emitted by the early Sun, seems capable of replicating observed He and Ne distributions. Grains carrying Q-gases possibly implanted by ion irradiation in a hot plasma subsequently experience large diffusive losses, primarily of He; Ne isotope ratios are essentially unaltered. At some later time they are exposed to radiation from the early sun that implants a post D-burning solar gas component, elevating the highly diffused $^{3}He/^{4}He$ and $^{4}He/^{20}Ne$ ratios with only minor effect on Ne since solar He/Ne is so high (Table S1). This scenario, while speculative, can reproduce the measured He and Ne compositions, including the anomalously low $^{4}He/^{20}Ne$ ratios.

Results of an example calculation are given in Table S1. Diffused Q-He and Q-Ne compositions were calculated by applying Fick's Law to a spherical grain initially uniformly loaded with Q-gases. In view of the mineral composition of the Track 41 particle given above, the grain was assumed to be dominantly metallic. The ratio of diffusion coefficients D(He)/D(Ne) was taken to be 10, an approximate value for diffusion from iron at temperatures of ~500-1000 K *(S12)*. With this ratio the diffusive loss factor $f(^{20}Ne)$ and fractionation of Ne isotope ratios from their values in the undiffused Q component are small (Table S1). The solar contribution to the final "Diffused Q + Solar" mixture is ~50% of the total ^{4}He but <1% of the total ^{20}Ne, so adding the solar component has little effect on Ne abundance and isotope ratios (Table S1). We have used the present solar-wind $^{3}He/^{4}He$ ratio in the calculation, but with higher diffusive He loss ($f(^{4}He)$ = 77) the lower estimate for the post D-burning ratio in the Sun (Fig. 2B, main text) can be accommodated. A final $^{4}He/^{20}Ne$ ratio of 10, an approximate average of the measured Stardust ratios, is obtained in this example; higher or lower degrees of Q-gas diffusion can replicate the observed range of ~1-20. The diffusion coefficient ratio D(He)/D(Ne) is constrained to be >5 for all solutions. With smaller ratios, Ne loss is large enough to fractionate $^{20}Ne/^{22}Ne$ to values below the Stardust measurement uncertainties.

Table S1. Comparison of Stardust measurements with He and Ne compositions generated by a mixture of diffused Q-gases with solar gases. The f(^{4}He) and f(^{20}Ne) entries are the factors by which the He and Ne initially present in the Q-carrier grain are diffusively depleted. Solar (solar wind) and undiffused Q compositions from Table 1, main text.

	^{3}He/^{4}He (x10^{-4})	^{20}Ne/^{22}Ne	^{21}Ne/^{22}Ne (x10^{-2})	f(^{4}He)	f(^{20}Ne)	^{4}He/^{20}Ne
Solar	4.44 ± 0.10	13.90 ± 0.08	3.35 ± 0.07			520 - 670
Undiffused Q	1.45 ± 0.15	10.10-10.70	2.78-2.94			110 ± 30
Diffused Q	0.876	9.88-10.46	2.75-2.91	47	2.2	4.9
Diffused Q + Solar	**2.75**	**9.90-10.49**	**2.75-2.91**			**10**
Stardust	**2.75 ± 0.21**	**10.55 ± 0.20**	**2.77 ± 0.14**			**~1-20**

References

S1. K. D. McKeegan *et al.*, *Science* **314**, 1724 (2006).

S2. A. J. Westphal *et al.*, *Meteorit. Planet. Sci.* 39, 1375 (2004).

S3. B. Marty, P. Robert, L. Zimmermann, *Meteorit. Planet. Sci.* 40, 881 (2005).

S4. R. L. Palma, R. O. Pepin, R. Becker, D. J. Schlutter, *Geochim. Cosmochim. Acta* **66**, 2929 (2002).

S5. R. L. Palma, R. O. Pepin, D. J. Schlutter, *Meteorit. Planet. Sci.* **40**, A120 (2005).

S6. A. O. Nier, D. J. Schlutter, *Rev. Sci. Instr.* **56**, 214 (1985).

S7. M. E. Zolensky *et al.*, *Science* **314**, 1735 (2006).

S8. S. A. Sandford *et al.*, Science **314**, 1720 (2006).

S9. L. P. Keller *et al.*, Science **314**, 1728 (2006).

S10. R. C. Reedy, in *Proc. 12th Lunar Planet. Sci. Conf., Geochim. Cosmochim. Acta* Suppl. **16**, pp. 1809-1823 (1981).

S11. C. M. Hohenberg, K. Marti, F. A. Podosek, R. C. Reedy, J. R. Shirck, in *Proc. 9th Lunar Planet. Sci. Conf., Geochim. Cosmochim. Acta* Suppl. **10**, pp. 2311-2344 (1978).

S12. H. Fechtig, W. Gentner, P. Lämmerzahl, *Geochim. Cosmochim. Acta* **27**, 1149 (1963).